
EXAFS Measurement of Iron bcc-to-hcp Phase Transformation in Nanosecond-Laser Shocks

Introduction

The dynamics of material response to shock loading has been extensively studied in the past.¹ The goal of those studies was to understand the shock-induced deformation and structural changes at the microscopic level. Laser-generated shocks have been recently employed² to broaden these studies to higher pressures (~ 100 GPa) and strain rates ($\sim 10^7$ to 10^8 s^{-1}). The use of *in-situ* EXAFS for characterizing nanosecond laser-shocked vanadium and titanium has been recently demonstrated.³ Additionally, the observed fast decay of the EXAFS modulations in titanium shocked to ~ 40 GPa was shown³ to be due to the α -Ti to ω -Ti phase transformation. We show that EXAFS can likewise be used to demonstrate the bcc-to-hcp phase transformation in iron. The great interest in this transformation stems from the fact that a significant part of the earth's core is thought to consist of hcp iron.⁴ Initially, Bancroft *et al.*⁵ showed that the multiple fronts propagating within shocked iron indicated a phase transformation at around 13 GPa. Subsequently, Jamieson and Lawson have shown,⁶ by diffraction in a diamond anvil cell, that a bcc-to-hcp phase transformation indeed occurs at around 13 GPa. The historical importance of this transition is that it was first observed under shocked, rather than static, compression. It also established the reliability of shocks for obtaining pressure-compression relations. The transformation has been extensively studied in gas-gun shock experiments^{7,8} using the velocity history of the back surface of the target, where a long (>10 ns) characteristic time for the transformation was deduced. This contrasts with the subnanosecond time derived in the present experiment. The longer times deduced from velocity measurements⁷ have been explained⁸ in terms of the pressure dependence of the characteristic time. Using Fig. 5 of Ref. 8, we can estimate a characteristic time for iron at a pressure of 35 GPa of ~ 5 ns. Much shorter times have been inferred from the residual microstructure that is quenched after the passage of nanosecond and even subnanosecond shocks.⁹ This observation of the transformation in nanosecond laser shocks confirms the latter finding. Unlike the evidence⁹ derived from the examination of residual microstructure after the experiment, the measurements here are *in-situ*.

The EXAFS spectrum of iron is markedly different in the bcc (or α -Fe) phase as compared with the hcp (or ϵ -Fe) phase;¹⁰ this provides a signature for identifying the transformation in laser-shock experiments. Transient phase-transformation experiments require methods for characterizing the crystal conditions (e.g., the pressure) during the transformation to substantiate the occurrence of the transformation. In static compression experiments, the temperature and pressure are independently controlled and measured. We show that the temperature and compression (and, hence, the pressure) can be deduced from the EXAFS record itself in addition to providing evidence of the phase transformation.

Experimental Setup

K-edge EXAFS measurements were performed on iron shocked to ~ 35 GPa with a 3-ns laser pulse, provided by 3 of the 60 beams of the OMEGA laser.¹¹ The radiation source for the EXAFS measurement was obtained by imploding a spherical target using the remaining 57 OMEGA beams. In a previous paper,¹² we showed that a CH shell imploded by a multibeam laser system emits intense and spectrally smooth radiation, lasting ~ 120 ps, and is suitable for EXAFS measurements on nanosecond time scales.

Figure 103.42 shows a schematic of the experimental configuration used to measure K-edge EXAFS absorption spectra in laser-shocked iron targets. Two cross-calibrated, flat-crystal spectrometers equipped with a Ge (1,1,1) crystal were used for measuring the incident and transmitted spectra on a single laser shot. The three shock-generating laser beams were stacked to form a 3-ns square pulse focused to an irradiance of 0.4 to 0.5 TW/cm². The delay time of the three-stacked beams, with respect to the remaining beams, was adjusted so that peak implosion (and emission) of the spherical target occurred just when the shock wave exited the metal layer. The planar target consisted of 8- μ m-thick polycrystalline iron foil (purity of 99.85%) coated on both sides with a 17- μ m-thick CH layer; thus, the iron layer is directly affected by the shock but not by the laser absorption and heating. A heat shield (1-mm-thick CH foil) minimizes the heating of the metal layer by the soft

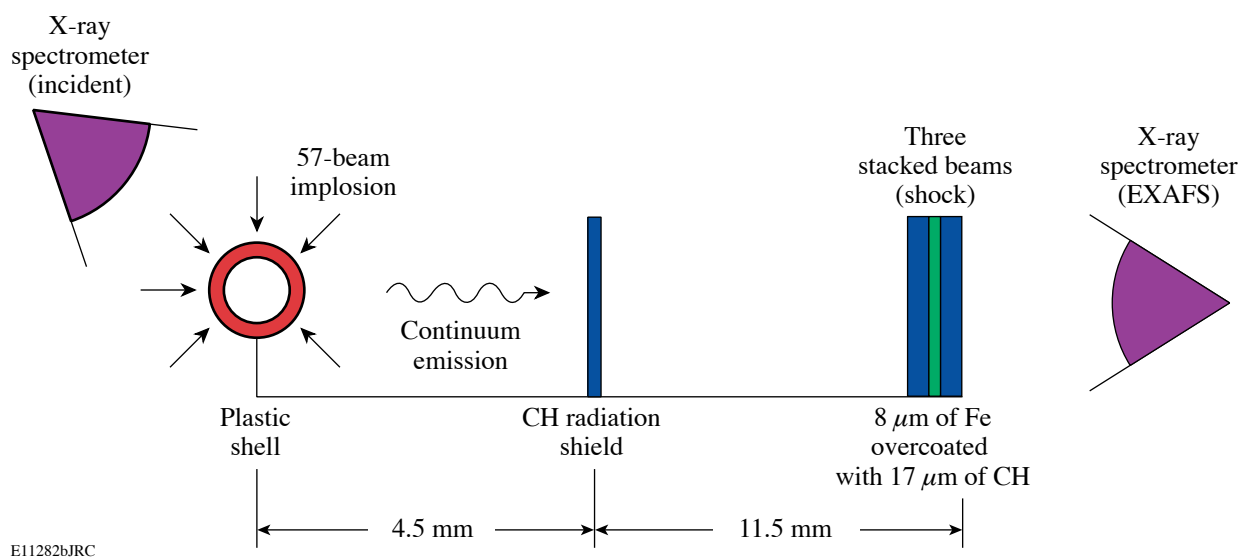


Figure 103.42

Schematic of the experimental configuration. The spherical target, imploded by 57 laser beams, serves as a radiation source for EXAFS measurements. The three-stacked beams launch a shock through the iron layer.

radiation from the imploding spherical target. The iron thickness is the largest that can still yield significant transmitted x-ray intensity. Although the spectrometers used in the EXAFS measurement are time integrated, a meaningful shock diagnosis can be obtained without streaking the spectrum in time because the x-ray pulse width is only ~ 120 ps,¹² much shorter than the shock transit time through the metal (\sim ns).

Theory

The expected shock strength and the properties of the shocked iron were determined using 1-D simulations with the hydrodynamic code *LASNEX*.¹³ The tabular equation of state incorporated into the code includes the α -Fe to ϵ -Fe phase transformation. Figure 103.43 shows the computed profiles just as the shock exits the iron layer. The volume-averaged values are a pressure of 36 GPa, a temperature of 645 K, and a compression of 1.2 (or 20%).

The measured spectra were analyzed with the FEFF8 *ab initio* EXAFS software package.¹⁴ The basic theory of EXAFS¹⁵ yields an expression for the relative absorption $\chi(k) = \mu(k)/\mu_0k - 1$, where $\mu(k)$ is the absorption coefficient and $\mu_0(k)$ is the absorption of the isolated atom. The wave number k of the ejected photoelectron is given by the de Broglie relation $\hbar^2 k^2 / 2m = E - E_K$, where E is the absorbed photon energy and E_K is the energy of the K edge. The FEFF8 package uses the scattering potential to calculate the amplitude and phase shift of the photoelectron waves scattered from several

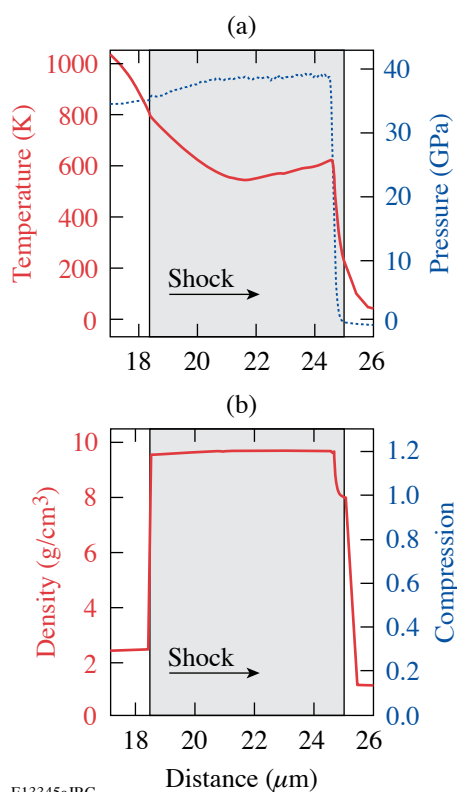
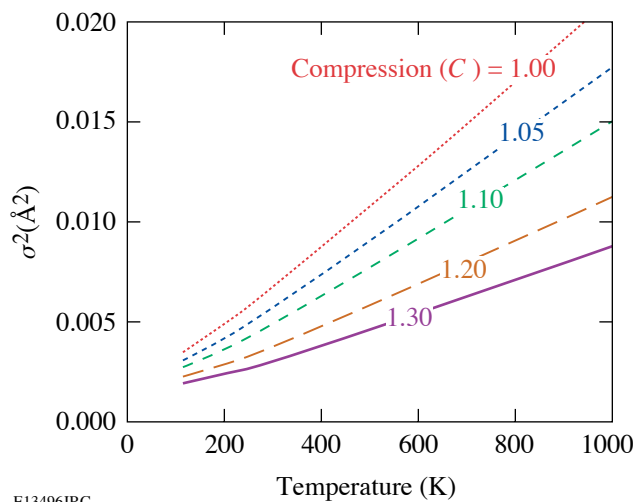


Figure 103.43

Profiles of (a) target pressure and temperature and (b) density calculated by *LASNEX* (the iron layer, enclosed within CH layers, is highlighted). The laser propagates toward the right.

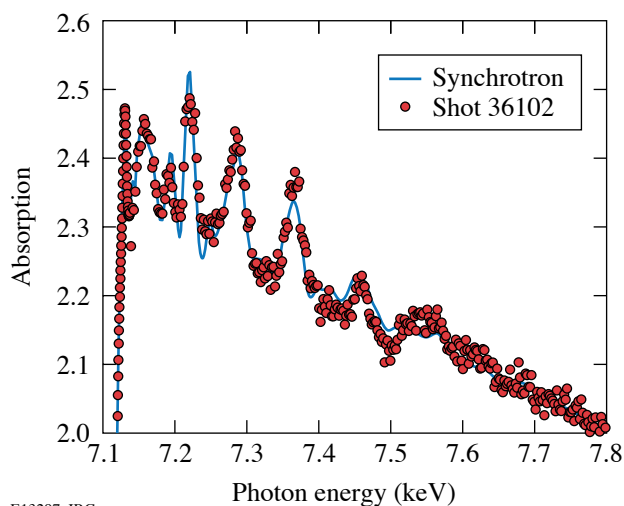
shells of neighboring atoms, including multiple-scattering paths. The main fitting parameters are the nearest-neighbor distance R and the vibration amplitude σ^2 appearing in the Debye–Waller term.¹⁵ The distance R yields the density or compression; σ^2 as a function of temperature was calculated using the Debye model¹⁶ for the phonon density of states, including correlation, and it also depends on the density through the



E13496JRC

Figure 103.44

Debye–Waller factor (σ^2) of ϵ -Fe, calculated from the correlated model of Sevillano *et al.*¹⁶ and the measured dependence of the ϵ -Fe Debye temperature on compression.¹⁷



E13297aJRC

Figure 103.45

Comparison of the measured absorption of unshocked iron on OMEGA and a standard iron EXAFS measured at the Stanford Synchrotron Radiation Laboratory.

Debye temperature. The density dependence of the Debye temperature for Fe- ϵ was taken from published measurements.¹⁷ The results (shown in Fig. 103.44) can be approximated by $\sigma^2(\text{\AA}^2) = 0.001 + 2 \times 10^{-5} T(K)/C^3$,⁵⁸ where $C = (\rho/\rho_0)$ is the compression ratio. Using this dependence and the result for σ^2 from FEFF8 fitting, the temperature can be derived.

Experimental Results and Analysis

To assess the reliability of our Fe EXAFS measurements, we obtained the EXAFS spectrum for unshocked iron using the configuration described above but without firing the shock-launching beams. Figure 103.45 shows a comparison between the resulting absorption and a standard iron absorption spectrum measured at the Stanford Synchrotron Radiation Laboratory (SSRL). The agreement is seen to be good.

EXAFS provides a very distinct, qualitative signature for the bcc-to-hcp phase transformation in iron.¹⁰ This is demonstrated by Fig. 103.46, showing (a) the EXAFS spectrum for the two phases calculated by the FEFF8 code and (b) the EXAFS spectrum measured on OMEGA for unshocked and shocked iron. Anticipating the fitting results described below, a compression of 20% (with respect to the initial bcc density) and a temperature of 700 K were assumed in Fig. 103.46(a) for the hcp phase. The bcc calculation is for room-temperature and ambient-pressure conditions. The main signature of the phase transformation is seen to be the disappearance of the peak marked “W.” When the calculations for the bcc phase are repeated for a wide range of compressions, the feature W remains intact. Thus, its disappearance can only be because of the phase transformation, not because of the shock compression (we later show that this is true—even in the case of 1-D compression). The effect of compression on the EXAFS spectrum is to increase the period of oscillation (in k space), and the effect of the heating is to cause the oscillations to decay faster with increasing k ; both are evident in Fig. 103.46(a).

The experimental results shown in Fig. 103.46(b) mirror the changes seen in Fig. 103.46(a). Compression and heating are evident, and the disappearance of the W feature indicates a bcc-to-hcp phase transformation. The complete disappearance of that feature indicates that the transformation is complete, hence that its time constant must be shorter than ~ 1 ns. Additionally, the predicted enhancement in the peak around $k \sim 3 \text{\AA}^{-1}$ is also observed in Fig. 103.46(b). These results were consistently observed on repeated experiments under the same conditions. These conclusions are borne out by the more precise fitting analysis below.

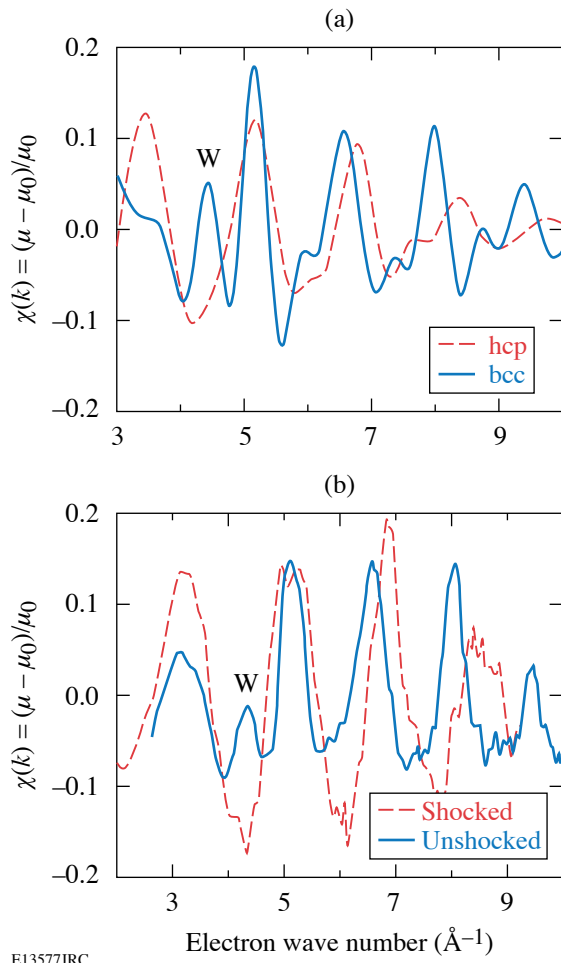


Figure 103.46

(a) FEFF8 code calculation of the EXAFS spectrum for unshocked α -Fe (bcc) and ϵ -Fe (hcp), the latter compressed by 20% with respect to the initial bcc iron. (b) Experimental results for unshocked and shocked iron. In the shocked case (at a deduced pressure of ~ 35 GPa), the peak marked W is seen to disappear, indicating a bcc-to-hcp phase transformation. Also, the period of oscillation is seen to increase, indicating compression. Finally, the damping rate increases, indicating heating.

To understand the origin of the W feature, we show the major components of the full EXAFS spectra calculated by the FEFF8 code for the bcc and hcp crystals in Fig. 103.47. The contributions from the first several shells of nearest neighbors, including several multiple scattering paths, are shown. Both crystals were assumed to be compressed by 20% and to have a temperature of 700 K. The calculation of a bcc crystal compression by 20% may seem unwarranted because the bcc phase is known to transform into the hcp phase at compressions above $\sim 6\%$. However, because of the much higher strain rate in this experiment, the phase transformation cannot be assumed *a priori* to take place. The origin of the W feature is seen to be a coincidence in the

waves scattered from the $n = 3$ and $n = 4$ shells occurring (for this compression) at $k \sim 4.7 \text{ \AA}^{-1}$. No such coincidence occurs for the hcp crystal. As mentioned before, the W feature is seen to remain intact even under compression. Thus, the disappearance of the W feature upon shocking in this experiment is not due to compression, but rather by phase transformation.

We now turn to FEFF fitting to the experimental EXAFS spectra. As Fig. 103.46 shows, we cannot fit the data with bcc EXAFS spectra; the two are qualitatively different. Conversely,

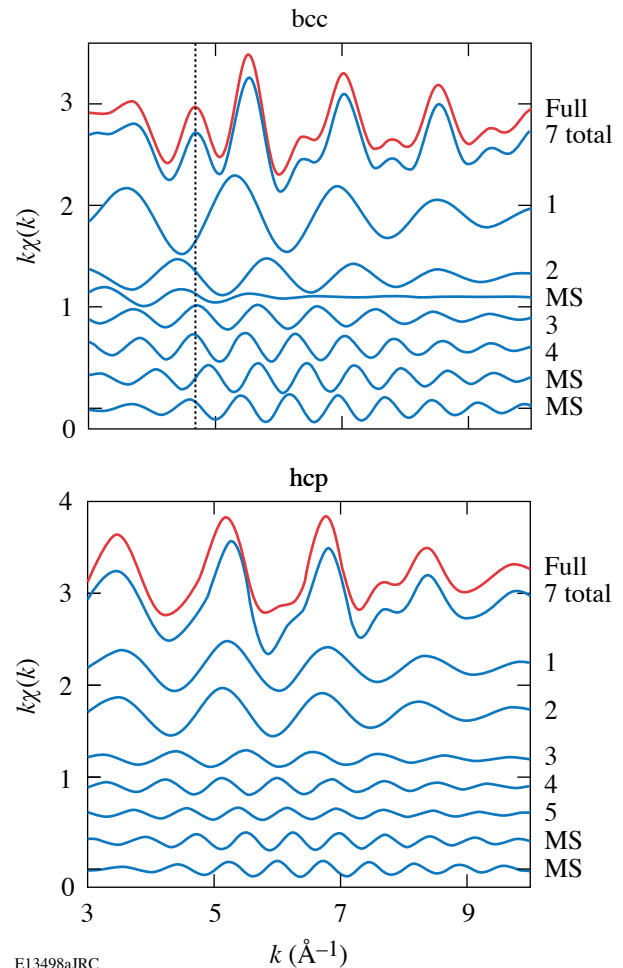
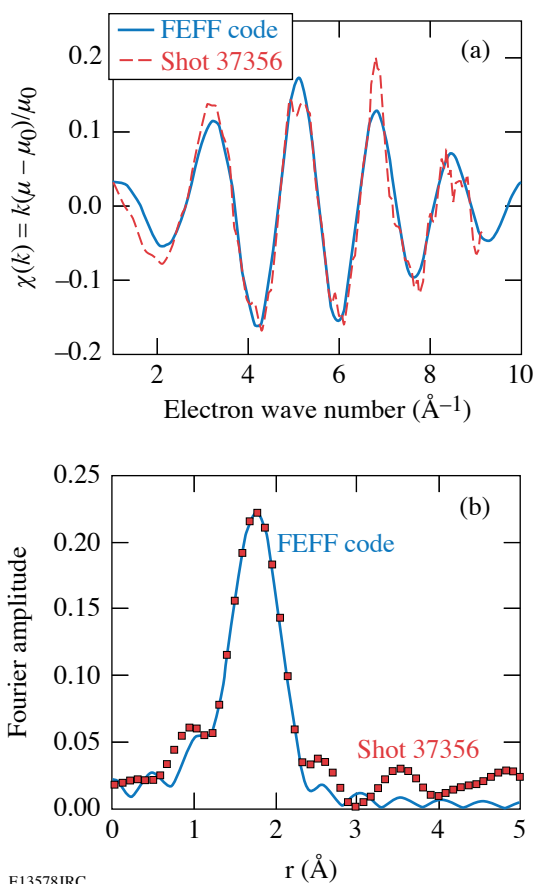


Figure 103.47

The major components of the FEFF-calculated EXAFS spectra due to scattering from the various shells of neighbors around the absorbing atom. The contributions of significant multiple scatterings are also shown ("7 total" is the sum of only the components shown in the figure). The peak marked W in Fig. 103.46 is marked here by a dotted vertical line. It is seen to arise from a coincidence in the scattering from the third and fourth shells at $k \sim 4.7 \text{ \AA}^{-1}$. Both crystals are assumed to be compressed by 20% and to be heated to 700 K.

hcp-calculated EXAFS agrees well with the experimental EXAFS data. Figure 103.48 shows the best fit, in wave number (k) space and in distance (r) space. The fit in r space (where the spectrum shows the spatial charge distribution around the absorbing atom) is obtained by inverse Fourier transforming the experimental, as well as the theoretical, curves in k space.¹⁵ The dimensions a and c of the hcp unit cell are known as a function of hydrostatic compression¹⁸ (for all compressions $c/a \sim 1.6$), and thus, the bond length (or nearest-neighbor distance) R is simply related to the compression under such conditions (we discuss the implications of finite shear strength below). Note that the value of R corresponding to the best fit is larger than the position of the peak in Fig. 103.48(b) because of the phase factors in the wave scattering. The fitting yields $R = (2.39 \pm 0.013) \text{ \AA}$, which corresponds to a compression of

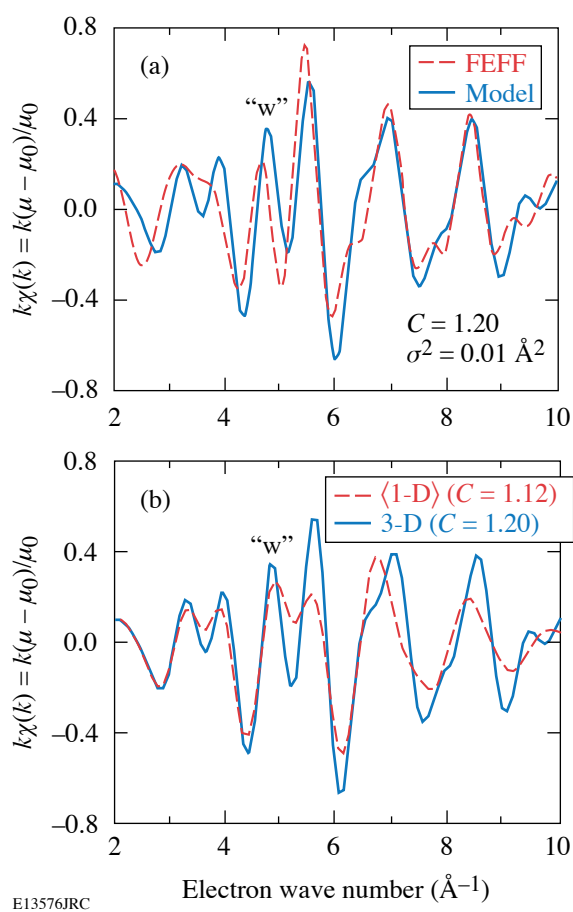


E13578JRC

Figure 103.48

FEFF code fitting to the experimental results (a) in the k space and (b) in the r space. The simulations assume the hcp phase. The best fit corresponds to a bond length of $R = (2.39 \pm 0.013) \text{ \AA}$ and $\sigma^2 = (0.0078 \pm 0.0030) \text{ \AA}^2$. These values correspond to a 20% volume compression and a temperature of 670 K.

1.22 ± 0.023 . This value agrees well with the average compression of 1.2 predicted by *LASNEX* [see Fig. 103.43(b)]. Turning now to the estimate of temperature, the FEFF best fit to the data [Fig. 103.49(a)] corresponds to $\sigma^2 = 0.0078 \pm 0.0030 \text{ \AA}^2$. From Fig. 103.44, this value of σ^2 corresponds to a temperature of $670 \pm 170 \text{ K}$, thus agreeing well with the average temperature of 645 K predicted by *LASNEX* [Fig. 103.43(a)]. Using the equation of state of iron and the measured temperature and compression values leads to an estimate of the pressure as $\sim 35 \text{ GPa}$. *LASNEX* uses the equation of state of iron, which includes the α to ϵ phase transformation (but not its kinetics). These values also agree with the equation of state calculated for the Hugoniot of iron.¹⁹ The deduced pressure is well above



E13576JRC

Figure 103.49

Simplified EXAFS calculations for 1-D and 3-D-compressed bcc iron. (a) Comparison of the simplified results and a full FEFF8 calculation for 3-D-compressed iron [$C = (\rho/\rho_0) = 1.2$, $T = 700 \text{ K}$]. (b) Two simplified EXAFS calculations: 3-D compression of $C = 1.2$ and 1-D compression of $C = 1.12$ (averaged over all directions). The compression in each case is adjusted to yield the measured EXAFS modulation frequency.

the pressure of slower shocks in iron, where a bcc-to-hcp phase transformation takes place.¹⁸ Also, the derived values of pressure and temperature correspond to a point on the phase diagram of iron⁵ that is well within the Fe- ϵ (hcp) region.

Velocity interferometric measurements (VISAR)²⁰ were performed on iron targets identical to those used for the EXAFS measurements, except that the CH coating was placed only on the side facing the laser. In this way, the velocity of the iron-free back surface could be measured. From the surface velocity, the particle velocity could be determined by dividing by 2. This relationship has been shown²¹ to hold for iron shocked to pressures of up to ~ 150 GPa. Because of the relatively high pressure and the small foil thickness in this experiment, the velocity waves^{7,8} indicative of a transition to plastic flow and of a phase transformation were not resolved; thus, the VISAR results cannot confirm either transition. However, the deduced particle velocity can be used with the known Hugoniot curve of iron to determine the compression. For the measured rear-surface velocity of 1.5×10^5 cm/s, the resulting compression is $C = 1.17$, in agreement with the values predicted by *LASNEX* and with the values measured by EXAFS (using the FEFF8-code fitting).

Elastic-to-Plastic Transition

The analysis above has assumed that the compression of the hcp crystal, but not necessarily that of the bcc crystal, is hydrostatic. The dynamic yield stress in polycrystalline iron has been found to be lower than 1 GPa,²² using millimeter-scale specimen thicknesses and strain rates of order of 10^5 s⁻¹. Because the dynamic yield stress in iron increases with strain rate as well as with decreasing specimen thickness,²² we cannot assume plastic compression of the bcc crystal prior to the phase transformation; in thin iron samples, the Hugoniot elastic limit can even be higher than the pressure for phase transformation.²³ However, the transformation involves atomic motions in various mutually perpendicular directions in the bcc phase,^{10,24} and thus, also in a direction perpendicular to the shock direction; this should lead to relaxation of the shear stress. In the hcp phase, the first shell of nearest neighbors, whose distance is given by the unit-cell parameter a , has a major contribution to the EXAFS spectrum; thus, the analysis primarily determines a , whereas the unit-cell parameter c is primarily needed for the calculation of volume compression. Therefore, values of c/a somewhat different from the static values used here cannot be excluded. However, such values would still imply a compression consistent within experimental error with the compression obtained by VISAR measurements and by hydrodynamic simulations.

Since the possibility of elastic compression of the bcc crystal cannot be discounted, the following question arises: Can the observed EXAFS be explained by a 1-D compression of the bcc crystal *with no* phase transformation? In other words: Would the W peak disappear because of 1-D compression where no phase transformation takes place? To answer this question, we calculated the EXAFS spectrum assuming that atomic coordinates in the bcc crystal are reduced only in the shock direction. Since the grains are oriented randomly in a polycrystalline sample, the angles between the crystal axes and the shock direction assume all possible values. Therefore, the result was averaged over all these angles. For simplicity, only single scattering from the first four nearest-neighbor shells was considered, using the scattering amplitudes and phase shifts from the tables of Teo and Lee.²⁵ To check the reliability of this model, Fig. 103.49(a) shows a comparison between the simplified and the full FEFF8 calculation for 20% isotropic compression of bcc iron at $T = 700$ K. Fair agreement between the two calculations is seen, and, in particular, the W feature appears in both. The W feature in both cases arises from the same coincidence of $n = 3$ and $n = 4$ scatterings. Figure 103.49(b) shows a comparison between the results for the cases of 3-D and 1-D compressions. The 3-D compression is 20%, as above. The 1-D compression was varied to match the experimental frequency of modulation, resulting in 12% compression (in slower shocks, the transformation starts to occur at a compression of $\sim 6\%$). This is larger than the reduction in distances in the 3-D case (which is $1.2^{1/3} \sim 1.06$) because in 1-D compression distances not in the direction of compression are reduced by a smaller factor. Since the W feature has not disappeared upon 1-D compression (nor has the first peak increased in intensity), the measured EXAFS spectra cannot be explained as resulting from a 1-D compression without a phase transformation. Thus, only the analysis assuming the hcp phase agrees with the measurement. As shown above, this conclusion agrees with VISAR measurements and *LASNEX* predictions.

ACKNOWLEDGMENT

This work was supported by the U.S. Department of Energy Office of Inertial Confinement Fusion under Cooperative Agreement No. DE-FC52-92SF19460, the University of Rochester, and the New York State Energy Research and Development Authority. The support of DOE does not constitute an endorsement by DOE of the views expressed in this article. Portions of this research were carried out at the Stanford Synchrotron Radiation Laboratory, a national user facility operated by Stanford University on behalf of the U.S. Department of Energy, Office of Basic Energy Sciences. Portions of this work were performed under the auspices of the U. S. Department of Energy by the University of California, Lawrence Livermore National Laboratory (LLNL) under Contract No. W-7405-Eng-48. Additional support was provided by LDRD project 04-ERD-071 at LLNL.

REFERENCES

1. J. E. Dorn and S. Rajnak, *Trans. Metall. Soc. AIME* **230**, 1052 (1964); U. F. Kocks, A. S. Argon, and M. F. Ashby, *Thermodynamics and Kinetics of Slip*, 1st ed., Progress in Materials Science, Vol. 19 (Pergamon Press, Oxford, 1975); M. A. Meyers and L. E. Murr, eds. *Shock Waves and High-Strain-Rate Phenomena in Metals: Concepts and Applications* (Plenum Press, New York, 1981).
2. B. A. Remington, G. Bazan, J. Belak, E. Bringa, M. Caturla, J. D. Colvin, M. J. Edwards, S. G. Glendinning, D. S. Ivanov, B. Kad, D. H. Kalantar, M. Kumar, B. F. Lasinski, K. T. Lorenz, J. M. McNaney, D. D. Meyerhofer, M. A. Meyers, S. M. Pollaine, D. Rowley, M. Schneider, J. S. Stölken, J. S. Wark, S. V. Weber, W. G. Wolfer, B. Yaakobi, and L. V. Zhigilei, *Metall. Mater. Trans. A* **35A**, 2587 (2004).
3. B. Yaakobi, D. D. Meyerhofer, T. R. Boehly, J. J. Rehr, B. A. Remington, P. G. Allen, S. M. Pollaine, and R. C. Albers, *Phys. Rev. Lett.* **92**, 095504 (2004); B. Yaakobi, D. D. Meyerhofer, T. R. Boehly, J. J. Rehr, B. A. Remington, P. G. Allen, S. M. Pollaine, and R. C. Albers, *Phys. Plasmas* **11**, 2688 (2004).
4. G. Steinle-Neumann *et al.* *Nature* **413**, 57 (2001).
5. D. Bancroft, E. L. Peterson, and S. Minshall, *J. Appl. Phys.* **27**, 291 (1956).
6. J. C. Jamieson and A. W. Lawson, *J. Appl. Phys.* **33**, 776 (1962).
7. L. M. Barker and R. E. Hollenbach, *J. Appl. Phys.* **45**, 4872 (1974).
8. J. C. Boettger and D. C. Wallace, *Phys. Rev. B* **55**, 2840 (1997).
9. C. S. Smith, *Trans. Am. Inst. Min. Pet. Eng.* **212**, 574 (1958); T. Sano *et al.*, *Appl. Phys. Lett.* **83**, 3498 (2003).
10. F. M. Wang and R. Ingalls, *Phys. Rev. B* **57**, 5647 (1998).
11. T. R. Boehly, R. S. Craxton, T. H. Hinterman, J. H. Kelly, T. J. Kessler, S. A. Kumpan, S. A. Letzring, R. L. McCrory, S. F. B. Morse, W. Seka, S. Skupsky, J. M. Soures, and C. P. Verdon, *Rev. Sci. Instrum.* **66**, 508 (1995).
12. B. Yaakobi, F. J. Marshall, T. R. Boehly, R. P. J. Town, and D. D. Meyerhofer, *J. Opt. Soc. Am. B* **20**, 238 (2003).
13. G. B. Zimmerman and W. L. Kruer, *Comments Plasma Phys. Control. Fusion* **2**, 51 (1975).
14. J. J. Rehr, R. C. Albers, and S. I. Zabinsky, *Phys. Rev. Lett.* **69**, 3397 (1992).
15. P. A. Lee *et al.*, *Rev. Mod. Phys.* **53**, 769 (1981).
16. E. Sevillano, H. Meuth, and J. J. Rehr, *Phys. Rev. B, Condens. Matter* **20**, 4908 (1979).
17. L. S. Dubrovinsky *et al.*, *Am. Mineral.* **85**, 386 (2000).
18. A. P. Jephcoat, H. K. Mao, and P. M. Bell, *J. Geophys. Res.* **91**, 4677 (1986).
19. R. G. McQueen *et al.*, in *High-Velocity Impact Phenomena*, edited by R. Kinslow (Academic Press, New York, 1970), Chap. VII, pp. 293–417.
20. P. M. Celliers *et al.*, *Appl. Phys. Lett.* **73**, 1320 (1998).
21. L. V. Al'tshuler *et al.*, *Sov. Phys.-JETP* **11**, 573 (1960).
22. R. W. Rohde, *Acta Metall.* **17**, 353 (1969).
23. G. E. Duvall, P. M. Bellamy, and R. J. Livak, in *Shock Waves and High-Strain-Rate Phenomena in Metals: Concepts and Applications*, edited by M. A. Meyers and L. E. Murr (Plenum Press, New York, 1981), Chap. 40, pp. 717–732.
24. V. P. Dmitriev, Y. M. Gufan, and P. Toledano, *Phys. Rev. B* **44**, 7248 (1991).
25. B.-K. Teo and P. A. Lee, *J. Am. Chem. Soc.* **101**, 2815 (1979).

